Detecting and Locating Broken Conductor Faults on High-Voltage Lines to Prevent Autoreclosing Onto Permanent Faults

Kanchanrao Dase, Sajal Harmukh, and Arunabha Chatterjee
Schweitzer Engineering Laboratories, Inc.

Detecting and Locating Broken Conductor Faults on High-Voltage Lines to Prevent Autoreclosing Onto Permanent Faults

Kanchanrao Dase, Sajal Harmukh, and Arunabha Chatterjee, *Schweitzer Engineering Laboratories, Inc.*

Abstract—Broken-conductor detection is challenging because the conductor may remain suspended without causing any fault current. Even if the conductor falls to the ground, the fault current might remain low, depending on the fault resistance. For low-resistance faults, a relay can detect faults and trip the line breakers. However, because the relay cannot determine whether the fault is permanent, it may attempt to reclose, causing further stress to the power system. This paper describes a new algorithm that uses only single-ended measurements to reliably detect broken conductors and estimate their location by using the charging current of the line. The phase angle of this current leads the voltage by about $\angle 90°$, and the magnitude is a function of line length. This method is suitable for power lines that have measurable charging current, and it detects broken conductors successfully if the relay can measure the charging current while the conductor is falling in midair. Broken-conductor detection can be used to trip the breakers before the conductor touches the ground and creates a shunt fault. Thus, the algorithm can prevent such faults and block any attempt to reclose the line. Detecting broken conductors and their location information provided by the algorithm can help in quickly resolving broken-conductor faults. This paper presents three field events from 57.1 kV and 220 kV lines and results from Electromagnetic Transients Program (EMTP) simulations that validate the algorithm.

I. INTRODUCTION

Transmission lines are exposed to a multitude of conditions that lead to the aging and weakening of conductors over time. According to [1], the aging mechanisms could be corrosion of aluminum or copper, galvanic corrosion, fatigue and fretting due to aeolian vibration, grease degradation, annealing, etc. In addition to aging, conductors are also exposed to localized damage or defects such as power-arcs, lightning strikes, hardware abrasion, gunshots, fires, tree strikes, etc. As a result, the conductors get corroded, bulge, or develop weak spots. If a damaged conductor is not repaired, it will eventually break, leading to a series fault.

It is important to note the typical sequence of events following the breaking of a conductor. Typically, as soon as the conductor breaks mechanically, arcing begins. As the distance between the broken segments of the conductor increases, the arcing eventually extinguishes and the conductor breaks electrically. Upon breaking, a conductor might remain hanging in the air or touch either the ground or the grounded supporting structure, causing a ground fault. Depending on the fault resistance, the fault may or may not produce enough current to facilitate detection by conventional protection. If the fault current is substantial, a relay might detect it and isolate the line.

The relay might also attempt to reclose on the broken and faulted line because it has not determined whether the fault is permanent. This is where broken-conductor detection becomes important. If the conductor break can be identified quickly (i.e., before the broken conductor falls to the ground and causes a fault) then not only can relays prevent the occurrence of a shunt fault by tripping the line, but they can also adaptively block autoreclosing onto permanent fault.

Commonly used broken-conductor detection methods rely on the amount of current unbalance crossing a certain threshold with some time delay. Current unbalance is most commonly calculated either as a ratio of the difference between the minimum and maximum phase currents to the maximum phase current or as the ratio of magnitude of the negative-sequence current to the positive-sequence current ($|I_2/I_1|$). Typically, the threshold for the current unbalance is kept at 20 percent with a large pickup delay (e.g., 5 to 60 seconds) for detection. This paper describes an algorithm for detecting broken conductors much more quickly.

The rest of this paper is organized as follows. Section II discusses the wide range of $|I_2/I_1|$ seen during broken-conductor events as well as the various factors affecting this ratio. Section III explains the challenges associated with using $|I_2/I_1|$ for broken-conductor detection. Section IV describes the proposed algorithm for detecting and locating broken-conductor faults. Section V and VI discuss the considerations for detecting broken conductors close to the relay and for lines with shunt reactors. Section VII covers simulation results, and Section VIII presents the field events. The paper conclusions are in Section IX.

II. $|I_2/I_1|$ AS SEEN FOR A BROKEN-CONDUCTOR EVENT AND THE FACTORS INFLUENCING IT

Fig. 1 illustrates the sequence network for a single-phase broken conductor, ignoring the shunt capacitances of the line. Using the current division rule, $|I_2/I_1|$ is calculated to be equal to $Z_{0Total} / (Z_{1Total} + Z_{0Total})$, where Z_{0Total} is the total zero-sequence impedance of the circuit (including local and remote sources and the line) and Z_{1Total} is the total positive-sequence impedance of the circuit. If we assume that, as typically seen, the total zero-sequence impedance is three times the total positive-sequence impedance, $|I_2/I_1|$ equals 0.75. Thus, for a single-phase broken-conductor event, we would expect $|I_2/I_1|$ to be around 0.75. However, there are scenarios where the total zero-sequence impedance might be much less than three times

the total positive-sequence impedance. This depends on the type of transformers connected at the sources. For example, a delta-wye-grounded transformer at the local source can cut off the zero-sequence impedance behind it, thus reducing the total zero-sequence impedance (see Fig. 2). This would significantly affect $|I_2/I_1|$.
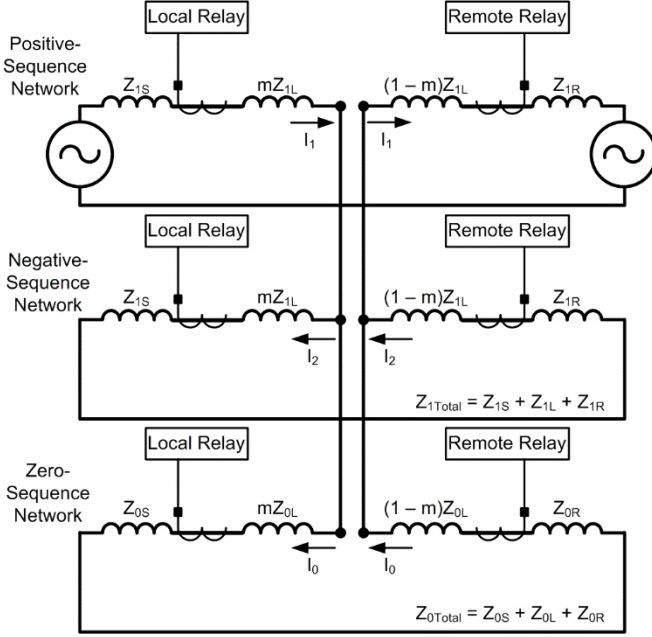
Fig. 1. Sequence network for a single-phase broken conductor at distance m from the local relay.
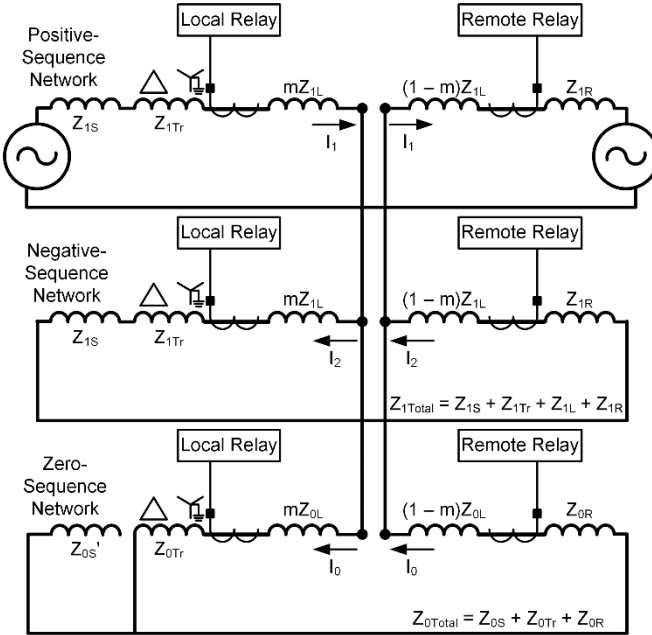
Fig. 2. Sequence network for a single-phase broken conductor with a delta-wye-grounded transformer at the local source.

Charging current also affects $|I_2/I_1|$ during low-load conditions. Consider the two-machine 132kV system as shown in Fig. 3. A transmission line of 75 mi, transposed every 25 mi, connects the two sources. This transmission line has a total charging current of about 34 A. The A-phase conductor is simulated to be broken 50 mi from the local end and remains

isolated with the ground path. Under this condition, $|I_2/I_1|$ is calculated and plotted in Fig. 4 by varying the voltage angle (δ) of the local source from 0.5° to 30°.
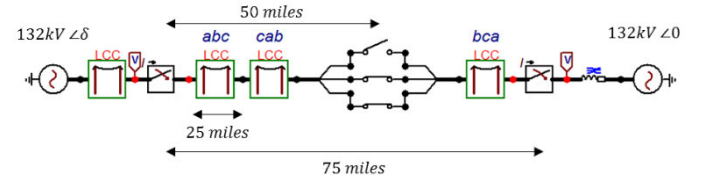
Fig. 3. 132 kV, two-machine system simulated in ATPDraw with a broken conductor 50 mi from the local relay.
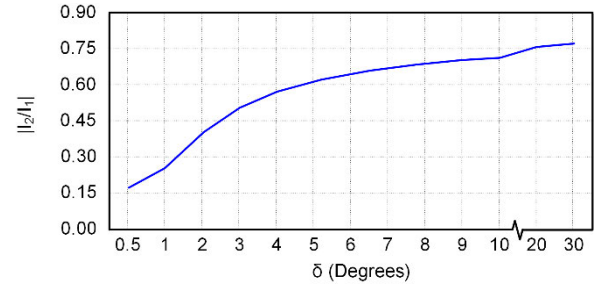
Fig. 4. $|I_2/I_1|$ under different loading conditions for the system shown in Fig. 3.

As shown in Fig. 4, for low-load conditions ($\delta < 3°$), $|I_2/I_1|$ is less than 0.5. This is because during low-load conditions, when the load current is comparable to the charging current, the load current is capacitive and balanced. When a conductor breaks in such a situation, the current for that phase does not change much, resulting in a relatively small negative-sequence current. However, as the load increases, the charging current of the broken conductor becomes negligible compared with the positive-sequence current magnitude and the ratio tends to follow $Z_{0Total} / (Z_{1Total} + Z_{0Total})$. For the system shown in Fig. 3, the value of $Z_{0Total} / (Z_{1Total} + Z_{0Total})$ is 0.78.

The load unbalance can also affect $|I_2/I_1|$, but for normal operating conditions, the amount of unbalance in transmission lines is low, so we can ignore this factor.

In summary, the proportion of the total zero-sequence impedance to the total negative-sequence impedance during a single-phase conductor break affects $|I_2/I_1|$. Further, $|I_2/I_1|$ becomes particularly sensitive under low-load conditions when the charging current of the broken-conductor phase is comparable (in magnitude) to the positive-sequence current. In such a case, $|I_2/I_1|$ can drop to as low as 0.1.

If conductors from two phases break, the negative-sequence current becomes equal to the positive-sequence current and $|I_2/I_1|$ equals 1. Thus, $|I_2/I_1|$ for a broken conductor in transmission lines can lie anywhere in the wide range of 0.1 to 1.

III. CHALLENGES IN BROKEN-CONDUCTOR DETECTION THROUGH USE OF $|I_2/I_1|$

The previous section showed that the range of possible values for $|I_2/I_1|$ is wide and detecting a broken conductor by using only $|I_2/I_1|$ is very challenging because the range of this ratio is not unique to broken-conductor events. Asymmetrical shunt faults within and beyond the zone of protection can also

have the $|I_2/I_1|$ ratio with values similar to broken-conductor events.

One way to differentiate between shunt faults and a broken conductor is to use a time-delayed operation for the broken conductor. Then we can expect the shunt faults to be cleared faster than broken conductors. But, because of time delays, the chances of preventing a shunt fault that might be caused by a broken conductor are slim.

Thus, detection using the $|I_2/I_1|$ method has many shortcomings:

- During low-load conditions, $|I_2/I_1|$ might drop to very low values, and $|I_2/I_1|$ might not cross the threshold value.
- A time delay in the order of seconds cannot prevent the possible occurrence of a shunt fault because of a broken conductor.
- The time coordination with upstream devices can be quite challenging for meshed systems where power flow can be bidirectional.
- It is difficult to achieve selectivity as elevated $|I_2/I_1|$ is seen at all locations upstream of the actual broken point.
- The direction of the broken point cannot be ascertained with just $|I_2/I_1|$, compromising protection security.

In Section IV, we present a new method that reliably detects the broken conductor before it falls to the ground and estimates the location by using line-charging currents.

IV. PROPOSED METHOD

The method this paper proposes relies on the charging current of the line for detecting broken conductors and is only suitable for lines that have significant charging current that the relay can reliably and accurately measure. Fig. 5 illustrates the flowchart for the algorithm. Four criteria have to be satisfied before the algorithm can declare a broken-conductor condition. The algorithm uses Criterion 5 to generate an alarm for uncertainty in broken-conductor detection during light loading conditions. This section describes these criteria and outlines the necessary calculations used in the algorithm.
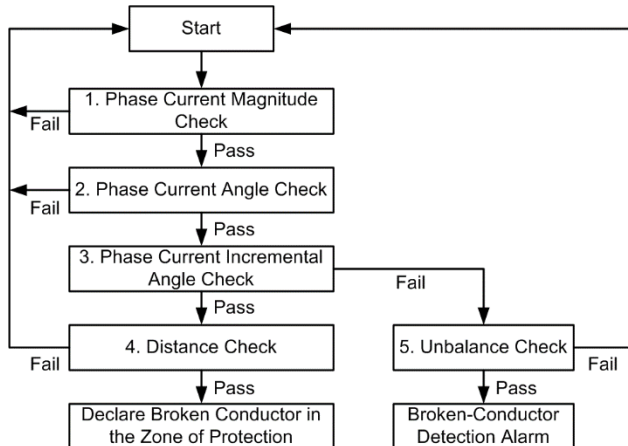
Fig. 5. Proposed algorithm flowchart for the detection of broken-conductor faults.

A. Phase Current Magnitude Check

This criterion is satisfied when the magnitude of the phase current becomes less than the total charging current for that phase; which is expected when a conductor breaks within the line length. For this, the algorithm requires information regarding the total charging current per phase, and there are various ways to obtain it. One way is to measure the steady-state current and the phase voltage magnitude while the line is being charged with the remote end open. Once the relay has these data, it can calculate the total charging current per phase for any real-time voltage because the charging current magnitude is directly proportional to the phase voltage magnitude.

Alternatively, the relay can calculate the approximate total charging current per phase by using (1).

$$\text{Total Charging Current Per Phase} = \frac{V_{ph}}{Z_{C1}} \tanh(\gamma_1 \bullet LL) \quad (1)$$

where:

V_{ph} is the phase voltage.

Z_{C1} is the positive-sequence characteristic impedance of the line given by $\sqrt{Z_1/Y_1}$.

γ_1 is the positive-sequence propagation constant of the line given by $\sqrt{Z_1 Y_1}$.

LL is the total transmission line length.

Z_1 is the positive-sequence impedance of the line length in pu.

Y_1 is the positive-sequence admittance of the line length in pu.

Equation (1) is derived from the long transmission line model [2]. Typically, in the case of a broken conductor, we expect that when the broken conductor is in midair and the initial arcing has extinguished, the current measured by the relay would be the capacitive charging current for the reduced line length (i.e., from the local relay until the point of breakage). This current would be less than the total capacitive charging current that would have been drawn by the whole length of that phase. If the current magnitude is greater than the total charging current for that phase, it implies that the conductor is not broken in the protected zone. However, if the measured phase current magnitude is less than the total charging current for that phase, it indicates that the line could be broken in the zone of protection. To include all possible cases of broken conductors over the length of the line, the phase current magnitude can be compared with a threshold of 110 percent of the total charging current for that phase. It is possible that the relay could measure no currents for close-in broken-conductor faults. For such scenarios, we use a different approach for detecting broken conductors, as explained in Section V.

B. Phase Current Angle Check

This criterion is satisfied if the phase current angle with respect to the corresponding phase voltage angle is verified to be within an expected range. For a broken conductor in isolation with any physical shunt path, the phase current

measured by the relay would be just about capacitive. Thus, the phase current angle would lead the phase voltage angle by about ∠90°. By setting a small window around ∠90° (e.g., ∠85° to ∠95°) we can filter the broken-conductor events and eliminate cases that indicate other conditions. Note that when the broken-conductor charging current has a low magnitude, the angle might go outside the window because of the line transposition and measurement errors. To take this into consideration, we can extend the ∠90° window (e.g., ∠80° to ∠100°) when the relay measures capacitive currents less than a certain magnitude (e.g., 20 percent of the total line-charging current). This gives more coverage to broken-conductor events and increases the dependability of the algorithm.

C. Phase Current Incremental-Angle Check

In very low-load conditions, the first two criteria might be satisfied without a conductor being broken. To make the algorithm more secure, we note the change in the phase current angle. We calculate this change in the current angle by subtracting the current angle measured upon satisfaction of the first two criteria from the current angle measured a certain time before that (e.g., 300 ms). This additional condition allows us to distinguish between low-load events that satisfy the first two criteria and broken-conductor events. Section IV.E. explains broken-conductor detection that uses unbalance check for low loads.

During normal operating conditions, the phase current and the phase voltage are related by the load angle. The current can be in phase, lagging, or leading the voltage phasor. After the conductor breaks and the arc extinguishes, the current starts leading the voltage phasor by approximately ∠90° as long as the conductor is in physical isolation with the ground path. For broken-conductor cases, the change seen in the current angle is in the counterclockwise direction for forward loads and in the clockwise direction for reverse loads, as shown in Fig. 6.
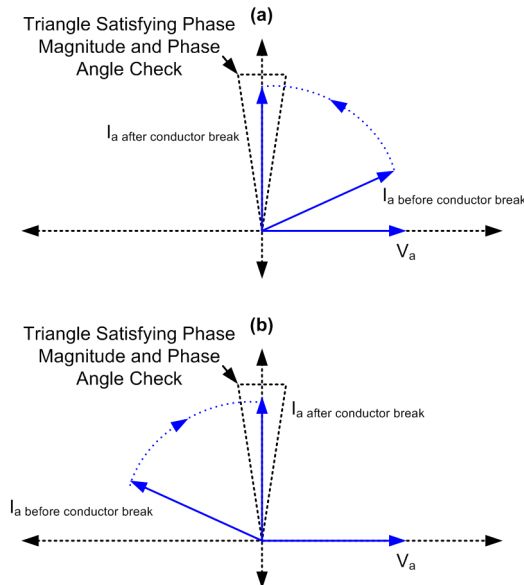
Fig. 6.   Relationship between A-phase current and voltage phasors before and after an A-phase conductor break for (a) forward power flow and (b) reverse power flow.

Thus, once the phase current magnitude and angle check criteria are satisfied, we can use the change in the phase current angle in a designated direction and by a particular threshold (such as ∠15°) as a metric to securely determine if the conductor is broken.

D. Distance Check

The final criterion in broken-conductor detection involves calculating the distance to the broken-conductor fault. If it is less than the line length or some set percentage of it (e.g., 95 percent), the last criterion is satisfied and the algorithm declares a broken-conductor fault within the zone of protection. If configured, we can use the algorithm output to trip the line breakers and block the autoreclose before the conductor falls on to the ground and creates a shunt fault.

We can calculate the distance from the relay terminal to the broken-conductor location in three different ways. The following subsections explain these calculations in detail.

1) Current Ratio Distance Calculation

This is the most simple way to calculate the distance from the relay terminal to the broken conductor. For a broken conductor, the relay measures the charging current up to the fault location (I_{break}) as long as the conductor is in physical isolation from the ground path and its corresponding phase voltage (V_{break}). Also, as explained in Section IV.A, the relay already has the total charging current per phase for the complete line length ($I_{total\ charging}$) for the corresponding phase voltage ($V_{total\ charging}$). With these two charging currents and their corresponding phase voltages, the relay can calculate the approximate distance to the broken conductor ($m_{current\ ratio}$), as shown in (2).

$$m_{current\ ratio} = \frac{I_{break}}{I_{total\ charging}} \cdot \frac{V_{total\ charging}}{V_{break}} \cdot LL \qquad (2)$$

where:

LL is the total transmission line length in mi or km.

2) Complete Equation Distance Calculation

For an A-phase broken conductor at distance m, the sequence network after the line breaks and the arc extinguishes can be represented in detail as shown in Fig. 7.

The red dashed-line arrows indicate the shunt capacitance charging currents of the distributed line model in different sequence networks. We can use long-line hyperbolic equations (3), (4), and (5) to estimate the sequence currents at distance m by using the local terminal sequence voltages and currents [2]. They are expressed as follows:

$$I_{1m} = I_{1L}\cosh(\gamma_1 m) - \frac{V_{1L}}{Z_{C1}}\sinh(\gamma_1 m) \qquad (3)$$

$$I_{2m} = I_{2L}\cosh(\gamma_1 m) - \frac{V_{2L}}{Z_{C1}}\sinh(\gamma_1 m) \qquad (4)$$

$$I_{0m} = I_{0L}\cosh(\gamma_0 m) - \frac{V_{0L}}{Z_{C0}}\sinh(\gamma_0 m) \qquad (5)$$
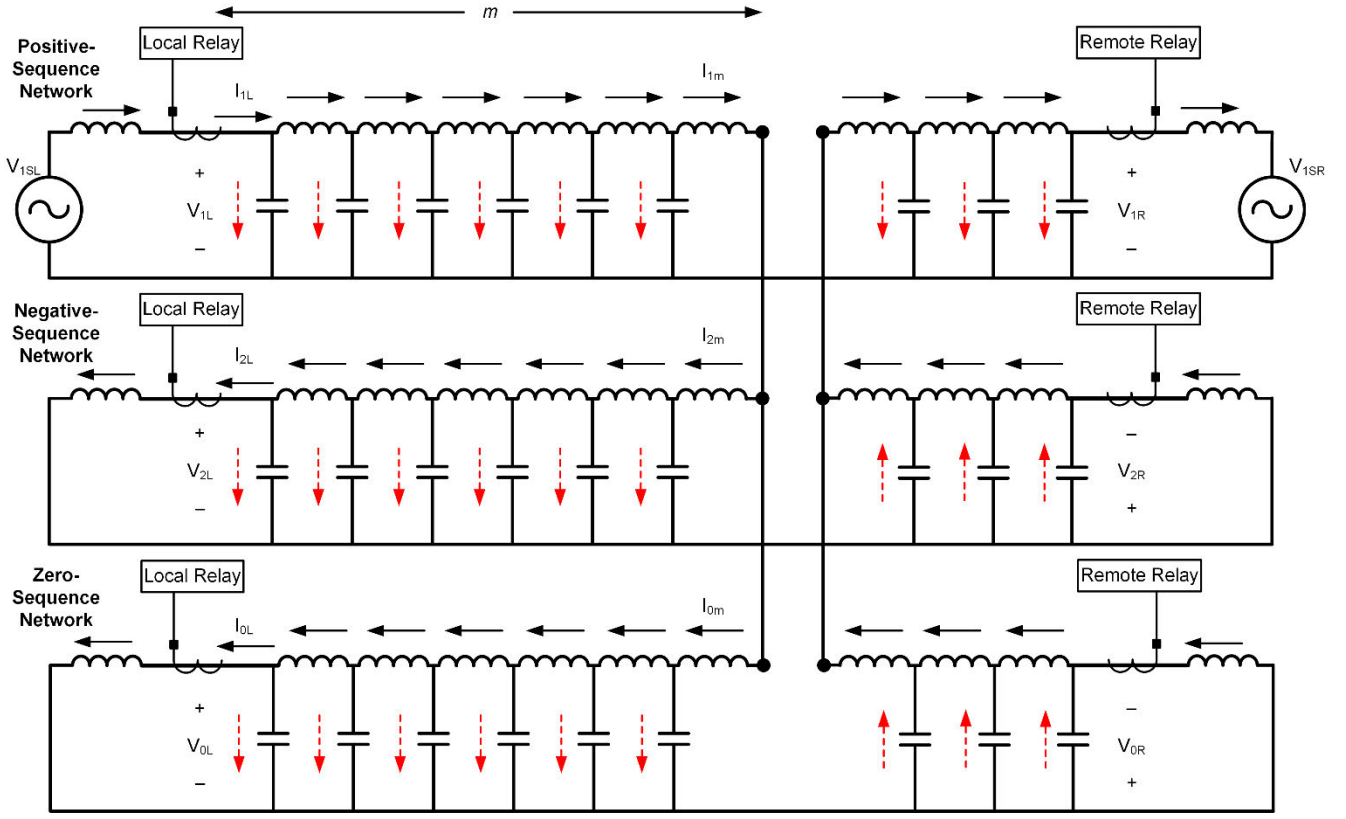
Fig. 7.   Detailed sequence network diagram for a broken conductor at distance *m* from the local relay.

The A-phase current at the broken-conductor location can be expressed as a sum of the positive-, negative-, and zero-sequence currents at that location ($I_{Am} = I_{1m} + I_{2m} + I_{0m}$) and can be equated to 0 (because the phase current is 0 at the point of breakage), as expressed in (6).

$$I_{Am} = I_{1L}\cosh(\gamma_1 m) - \frac{V_{1L}}{Z_{C1}}\sinh(\gamma_1 m) +$$

$$I_{2L}\cosh(\gamma_1 m) - \frac{V_{2L}}{Z_{C1}}\sinh(\gamma_1 m) + \qquad (6)$$

$$I_{0L}\cosh(\gamma_0 m) - \frac{V_{0L}}{Z_{C0}}\sinh(\gamma_0 m) = 0$$

Adding and subtracting $\left[I_{0L}\cosh(\gamma_1 m) - \dfrac{V_{0L}}{Z_{C0}}\sinh(\gamma_1 m) \right]$

to (6) and further simplifying, the resulting equation is expressed as (7).

$$I_{Am} = \left[I_{AL}\cosh(\gamma_1 m) - V_{AL}\left(\frac{\sinh(\gamma_1 m)}{Z_{C1}} \right) \right] +$$

$$\left\{ I_{0L}\left[\cosh(\gamma_0 m) - \cosh(\gamma_1 m) \right] - \qquad (7)$$

$$V_{0L}\left[\left(\frac{\sinh(\gamma_0 m)}{Z_{C0}} \right) - \left(\frac{\sinh(\gamma_1 m)}{Z_{C1}} \right) \right] \right\} = 0$$

where:

I_{Am} is the current of the broken-conductor phase at distance *m* from the local terminal.

m is the distance in mi or km to the broken conductor.

I_{AL} is the current of the broken-conductor phase at the local terminal.

I_{0L} is the zero-sequence current at the local terminal

V_{AL} is the voltage of the broken-conductor phase at the local terminal.

V_{0L} is the zero-sequence voltage at the local terminal

Z_{C1}, γ_1, Z_1, and Y_1 are as defined in Section IV.A.

Z_{C0} is the zero-sequence characteristic impedance of the line given by $\sqrt{Z_0/Y_0}$.

γ_0 is the zero-sequence propagation constant of the line given by $\sqrt{Z_0 Y_0}$.

Z_0 is the zero-sequence impedance of the line length in pu.

Y_0 is the zero-sequence admittance of the line length in pu.

Equation (7) does not have a closed-form solution for distance *m*, and we must use an iterative approach to obtain it. The solution from (7) assumes that the lines are perfectly transposed and uses zero-sequence parameters, which may not be accurately known because of changing weather conditions and variations in the zero-sequence return paths in the ground.

In summary, (7) is computationally inefficient, and the calculated distance *m* has errors because of the untransposed nature of the line and its dependence on zero-sequence parameters.

3) Positive-Sequence Distance Calculation

We can break (7) into two parts: P1 (8) and P2 (9), as follows.

$$P1 = I_{AL} \cosh(\gamma_1 m) - V_{AL}\left(\frac{\sinh(\gamma_1 m)}{Z_{C1}}\right) \tag{8}$$

$$P2 = I_{0L}\left[\cosh(\gamma_0 m) - \cosh(\gamma_1 m)\right] - V_{0L}\left[\left(\frac{\sinh(\gamma_0 m)}{Z_{C0}}\right) - \left(\frac{\sinh(\gamma_1 m)}{Z_{C1}}\right)\right] \tag{9}$$

From the simulation results in Section VII.D, we see that the distance *m* calculations using the complete equation method from (7) and (8) are almost the same. This means that (9) has a negligible effect on the outcome of the distance *m* calculation and can be ignored in (7). Thus, removing P2 from (7), we get (10).

$$I_{AL}\cosh(\gamma_1 m) - V_{AL}\left(\frac{\sinh(\gamma_1 m)}{Z_{C1}}\right) = 0 \tag{10}$$

Simplifying further, (10) can be solved for distance *m*, and it can be expressed as follows:

$$m = \frac{1}{\gamma_1}\tanh^{-1}\left(\frac{I_{AL} \bullet Z_{C1}}{V_{AL}}\right) \tag{11}$$

Equation (11) assumes perfectly transposed transmission lines, so it would have slight errors because of the untransposed nature of the line. However, unlike (7), (11) uses only the positive-sequence parameters that are likely to be accurately known compared with the zero-sequence parameters. Further, (11) gives a closed-form solution for distance *m*, thus making it more computationally efficient because we do not need iterations.

E. Unbalance Check

In some broken-conductor cases, it is possible that the first two criteria (magnitude and angle checks) pass but the third criterion (incremental-angle check) fails. For instance, consider an energized line with a very light load such that the first two criteria are satisfied. If there is a broken-conductor fault in the protected line length, the third criterion might not be satisfied. This is because the current phasor angle change, before and after the fault, might not be greater than the set threshold (e.g., $\angle 15°$). So, even though it is a broken-conductor fault, we cannot make a definitive declaration because it might also be a case of load change on that phase. Thus, for these cases, the algorithm initiates an alarm if the unbalance through the use of $|I_2/I_1|$ is greater than the set threshold (e.g., 0.25). Note that the pickup threshold should be greater than the standing unbalance of the line. However, if we are certain that there are no such unbalance load changes in the system, we can use the first two criteria (i.e., magnitude and angle checks) along with the

unbalance and the distance checks for tripping. Note that the unbalance check may fail to assert when the conductor breaks around the remote terminal that has very low or no load.

V. CONSIDERATIONS FOR CLOSE-IN BROKEN-CONDUCTOR FAULTS

When a conductor breaks very close to the relay location, the charging current measured by the relay is negligible. The relay cannot calculate angles of such small magnitudes of currents because the phasor cannot be accurately determined, so we cannot evaluate the phase angle and phase incremental-angle checks of the proposed algorithm. To detect broken conductors under such scenarios, we must use a different approach.

Consider Transmission Line 1 in Fig. 8 being protected for broken-conductor faults. Line 1 is connected to the bus through disconnectors and the breaker. The bus is also connected to other feeders and a transformer, which is typical for transmission systems. The relay declares a broken-conductor fault when the relay measures current magnitude close to zero in any of its phases and the following conditions are true:

- Relay measures healthy phase voltages on the protected line.
- The protected line has measurable charging current over the entire length.
- If there is a shunt reactor locally connected to the protected line, the reactor current is compensated to calculate the actual current flowing into the line.
- The disconnectors and breakers of all the phases of the protected line are closed. This indicates that the protected line is connected to the bus.
- The bus is not being energized.
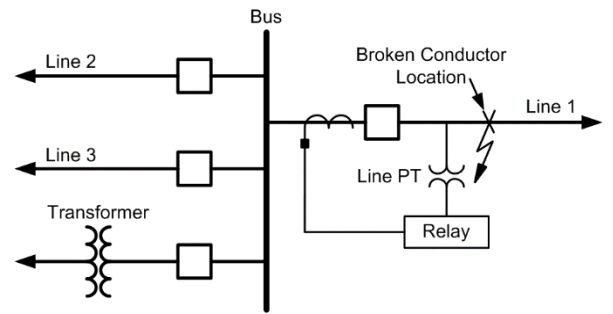
Fig. 8.   One-line diagram of a typical transmission substation with a close-in broken-conductor fault on Line 1.

Thus, if the relay measures current magnitudes close to zero in any of the protected line phases and all the above conditions are satisfied, we can declare with certainty a close-in broken-conductor fault for those phases.

VI. CONSIDERATIONS FOR LINES WITH SHUNT REACTORS

The proposed logic for detecting broken conductors can be slightly modified when there is a shunt reactor at the end of the line, as shown in Fig. 9. If the line is energized from the local end with the remote breaker open, the charging current measured by the relay will be less than the charging current of the same line with no shunt reactor. The decrease in charging

current is because of consumption of VARs by the shunt reactor drawing the shunt capacitive current of the line.
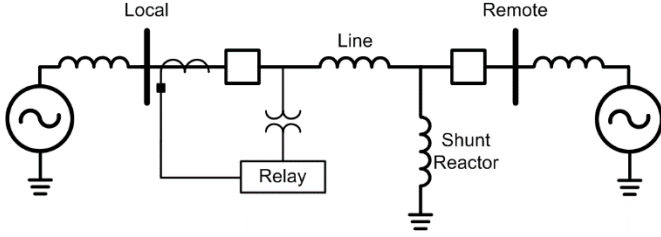
Fig. 9.   Transmission line with a shunt reactor at the remote end.

For the system shown in Fig. 9, assume that the shunt reactor connected to the protected line compensates for 40 percent of the total VARs generated by the line. Consider the A-phase total charging current without a shunt reactor to be 100 A and with a shunt reactor to be 60 A, as illustrated in Fig. 10. Now, two possibilities arise when the local relay measures 60 A of capacitive current in any of its phases—there could either be a broken-conductor fault at 60 percent of line length from the local relay or a pole-open condition or broken conductor at the remote end with the shunt reactor connected to the line. Thus, for lines with shunt reactors, the proposed algorithm needs to be modified to take into account the various conditions that create the same effect.
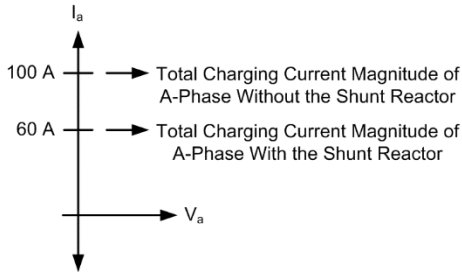
Fig. 10.   A-phase charging current magnitudes with and without shunt reactors for the transmission line in Fig. 9.

We assume that the protected line with the shunt reactor is terminated to a bus that has more than one feeder or transformers connected to it, which is typical for transmission systems. If the remote-breaker status is not available, the broken-conductor algorithm executes as-is unless the relay measures a capacitive current around the total charging current of the line with shunt reactors. If it does, the relay issues an alarm instead of a trip because a remote-end, pole-open condition may also create this scenario. For example, in the example described above, if the capacitive current measured by the relay is around 60 A (e.g., 55 A to 65 A) and all the criteria of the proposed algorithm are satisfied, the algorithm issues an alarm. However, if the remote-breaker status is available, we can make the algorithm more dependable for such scenarios by using the unbalance current check (i.e., the relay can issue a trip when the unbalance check is satisfied with all the remote-breaker poles closed). Unbalance check is necessary because the relay can still measure currents equal to the charging current of the line with shunt reactors when the remote breakers are closed with no load.

VII.   SIMULATION RESULTS

We ran various Electromagnetic Transients Program (EMTP) simulations using ATPDraw and MATLAB to verify the proposed algorithm for broken-conductor faults in single- and double-circuit nonhomogeneous systems. This section outlines the simulation models and presents the results of an A-phase broken-conductor event simulated every 5 mi along the length of the line, including 0 and 100 percent of the line. The single-circuit model, as shown in Fig. 11, uses a 132 kV transmission line of 90 mi. The source angle difference between local and remote sources for this system was kept at ∠20°. The double-circuit model, shown in Fig. 12, uses 220 kV parallel transmission lines of 135 mi. The source angle difference between local and remote sources for this system was kept at ∠24°. Both the single-circuit and double-circuit line models have a single conductor per phase, transposed every 45 mi. Appendix A provides additional technical details about these models.
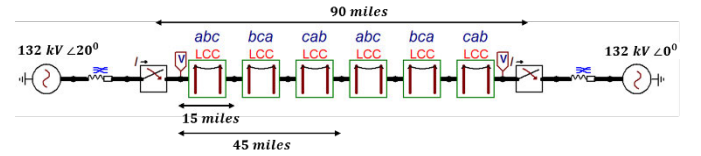
Fig. 11.   Single-circuit line simulation model.
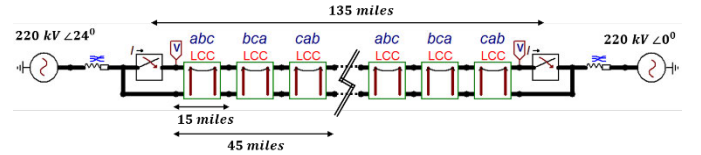
Fig. 12.   Double-circuit line simulation model.

The following subsections present and compare the simulation results for all the criteria discussed for the proposed algorithm in Section IV.

A.   Phase Current Magnitude Check

The relay records the charging current of the total line when the line is energized and breakers at the remote end are open. Ideally, we expect the charging current of the line to be the same whether energized from the local or remote end. But in reality, the charging current is a function of source impedance because it affects the terminal voltage. For simplicity, we only noted the maximum of the local or the remote charging currents. In the double-circuit line model, the parallel and the protected lines are energized together from either end, and the relay records the steady-state charging current. This means that when the charging current of the protected line is measured, there is no load on the parallel line.

The charging currents noted for single- and double-circuit models are then scaled up by 1.1 (110 percent of the protected line) and used as a threshold value to compare the phase current magnitude. Alternatively, the charging current can also be calculated using (1). The threshold values obtained for single- and double-circuit lines are as follows:

Single-circuit threshold current: 46 A

Double-circuit threshold current: 123 A

These values are indicated in Fig. 13 as the topmost flat portion. The charging currents measured for the A-phase conductor as broken-conductor events are simulated at various locations over the length of the line and are plotted with reference to the A-phase voltage in Fig. 13a for a single-circuit line and Fig. 13b for a double-circuit line. These figures show that the magnitude of the broken-conductor charging current is always below the threshold current, thus satisfying the phase current magnitude check.
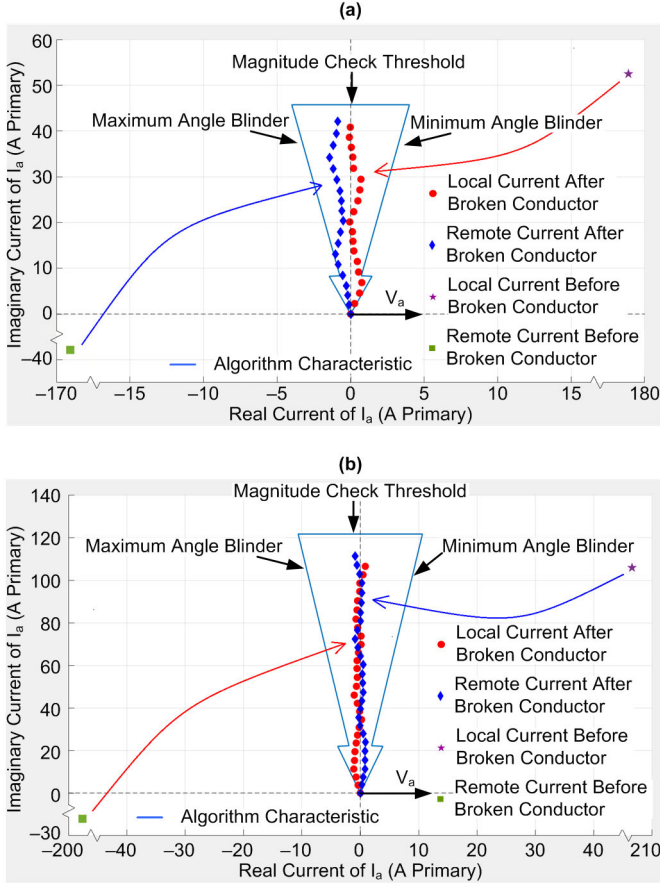
Fig. 13.   A-phase current vectors with respect to A-phase voltage plotted before and after the conductor breaks over the length of the line for (a) single-circuit model and (b) double-circuit model.

B. Phase Current Angle Check

The algorithm compares the current angle of the three phases with respect to the corresponding phase voltage to a window around $\angle90°$. For the simulation studies, we chose a window of $\angle85°$ to $\angle95°$. This angular window, along with the magnitude threshold, is plotted in the complex plane as the algorithm characteristic. The interior of this region can be considered the operating zone and the exterior can be considered the restraining zone for the broken-conductor fault. We see that at small current magnitudes (less than 10 A for single-circuit models and 20 A for double-circuit models), the angles spread out of the window because of line transposition errors. The angle blinders are expanded by $\angle5°$ on either side below those current magnitudes to improve dependability. Fig. 13 illustrates that the phase current angles for all broken-conductor faults fall inside this region, thus satisfying the phase current angle check.

C. Incremental-Angle Check

We used an incremental-angle threshold of $\angle15°$ to test the security of the broken-conductor fault detection. Before a broken-conductor fault occurs, the phase currents are related to the phase voltages by the load angle. After the conductor has broken and the arc is extinguished, the current in the broken-conductor phase leads the phase voltage by approximately $\angle90°$. Thus, if the current angle after a conductor break changes by more than $\angle15°$ clockwise for reverse power flow or counterclockwise for forward power flow, then the incremental-angle check would pass. Fig. 13 shows that the incremental-angle value is more than $\angle50°$ for all cases, and the change is in the expected direction, so this criterion passes.

Note that this change in current angle is heavily dependent on the pre-fault loading conditions, and therefore, the incremental-angle threshold should be carefully set to ensure that most of the cases are taken into account.

D. Distance Check

Per the proposed algorithm, we can calculate the distance to the broken-conductor fault through three different methods: current ratio, complete equation, and positive-sequence. The associated errors are presented and compared in Fig. 14 and Fig. 15.
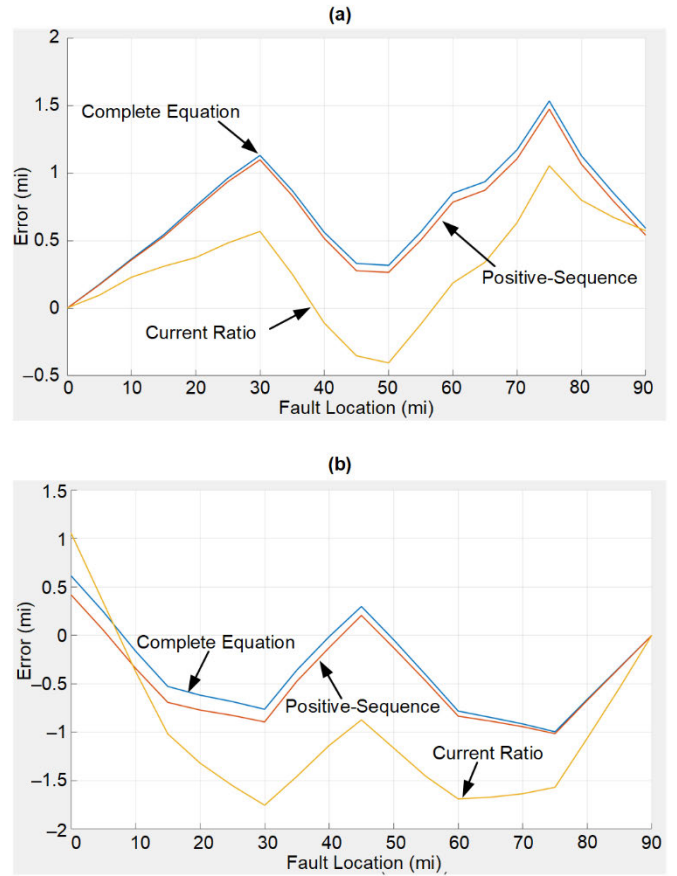
Fig. 14.   Errors in the distance to the broken-conductor fault location when using the current ratio method, positive-sequence method, and complete equation method for the single-circuit model from (a) the local end (b) the remote end.
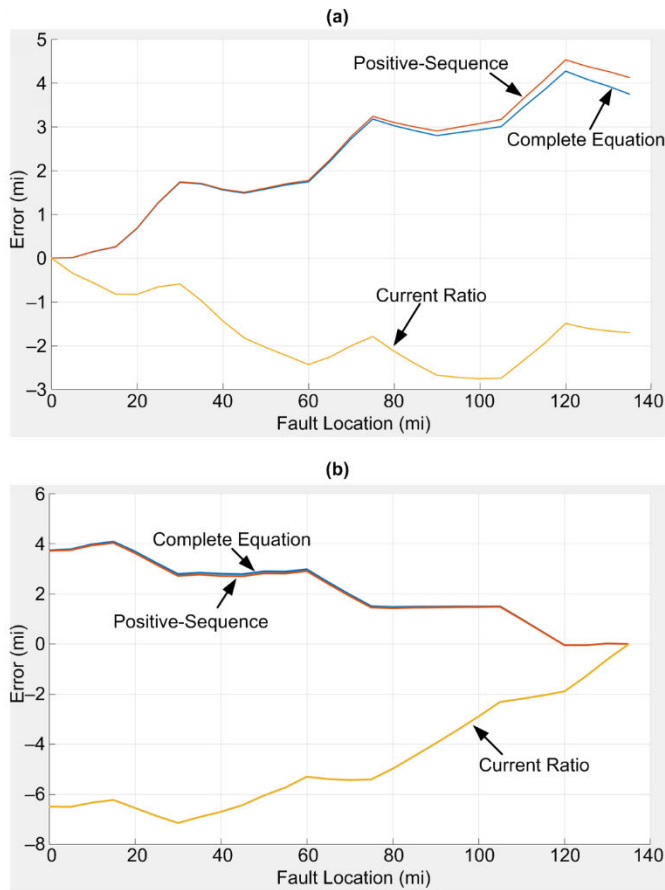
Fig. 15. Errors in the distance to the broken-conductor fault location when using the current ratio method, positive-sequence method, and complete equation method for the double-circuit model from (a) the local end (b) the remote end.

Fig. 14 plots the error in distance calculation for a single-circuit line by using the three methods for local and remote relays. The maximum error found was approximately 1.8 mi, and it was found when using the current ratio method. The errors in all three methods are mainly because of the untransposed nature of the line. We can also see from Fig. 14 that the errors between the complete equation and the positive-sequence methods are very small and are in the order of only one-tenth of a mile and can be ignored for all practical purposes.

Fig. 15 plots the error in distance calculation for a double-circuit line by using the three methods for local and remote relays. The maximum error in this case is around 7 mi, which was again using the current ratio method. Note from Fig. 15 that for all methods, the errors increase from one end to the other. This is because of increased mutual interaction between the protected line and the parallel line over the length of the line.

The errors when using the positive-sequence and complete equation methods were found to be less than 4.5 mi over the length of 135 mi and tend to underreach, enhancing security. However, the current ratio method may underreach or overreach depending on the loading of the parallel line. The errors between the positive-sequence and complete equation methods are less than half a mile.

E. Unbalance Check

The unbalance check generates a broken-conductor alarm when the incremental-angle check fails. From simulations, we calculated the magnitude ratio of I_2/I_1 for broken-conductor faults over the length of the line. Fig. 16 illustrates the $|I_2/I_1|$ ratio for both single-circuit and double-circuit lines as seen by local- and remote-end relays. As we see from the figure, the ratio varies over a wide range (0.5–0.9), even with considerable loading (load angles of $\angle 20°$ and $\angle 24°$) between the two machines in the single-circuit and double-circuit models.
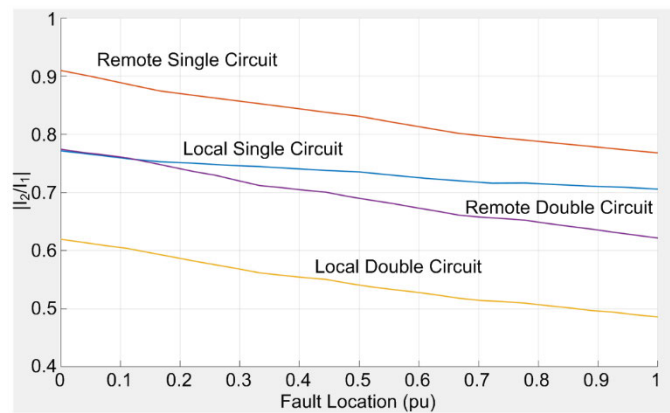
Fig. 16. $|I_2/I_1|$ for broken-conductor faults over the length of the line for single-circuit and double-circuit models.

VIII. FIELD EVENTS

This section describes three broken-conductor field events that occurred on different line configurations and illustrates how the proposed algorithm works.

A. Field Event 1: C-phase Broken-Conductor Event on a 220 kV Transmission Line

This section describes a broken-conductor event that occurred on a 144 km, 220 kV transmission line. In this event, the C-phase conductor of the line broke about 8 km from the local end. The section of the broken conductor from the local end remained hanging in the air while the section from the remote end fell to the ground, creating a shunt fault. See Fig. 17 for a visual representation.
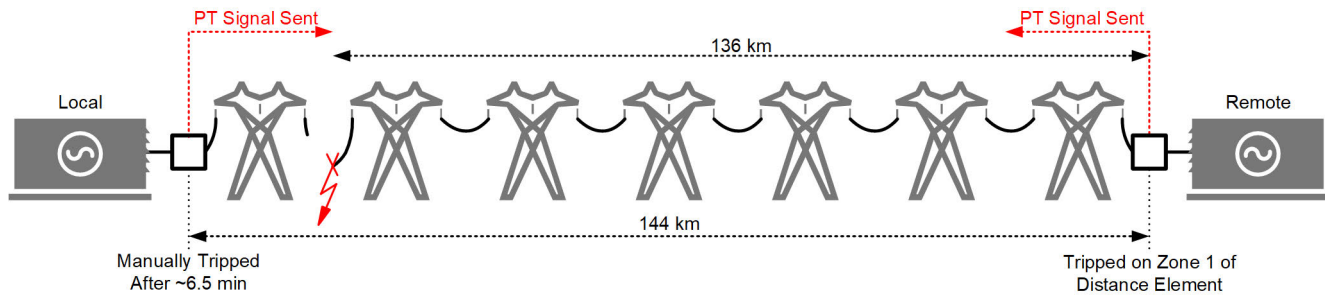
Fig. 17.   Broken-conductor field event on a 220 kV transmission line.

One of the schemes used to protect the line was permissive overreaching transfer trip (POTT), as shown in Fig. 18.
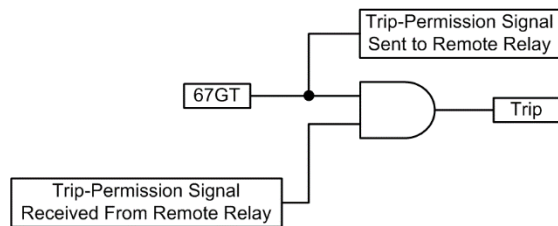
Fig. 18.   POTT scheme used for line protection.

The scheme was configured to trip the line breakers when the time-delayed ground directional-overcurrent element (67GT) picked up and the relay received a trip-permission signal from the remote-end relay. Additionally, the relay was configured to send a trip-permission signal to the remote-end relay once 67GT picked up in the relay (see Fig. 18).

1)   The Sequence of Events From the Local End

Fig. 19 shows the current waveform of the broken conductor phase captured by the local relay at the rate of 960 samples per second. Fig. 19a includes two consecutive time-separated reports of the same event. They are separated by a gap of 46 ms during which no data were captured.

We see from Report 1 in Fig. 19a, that the relay measured a continuous drop in the current amplitude. This is most likely because of the increasing series arc resistance while the two segments of the broken conductor were falling apart. After about 270 ms from the start of the conductor physical break, the resistance between the ends of the falling segments became significant enough to break the series arc. The zero-crossing point of the current waveform at which the arc was most likely extinguished is labeled as the arc breaking point in Fig. 19a. The current measured by the local relay after the arc breaking point is capacitive because it leads the C-phase voltage around $\angle 90°$, as shown in Fig. 19c. This only occurs if the conductor breaks electrically and is in physical isolation with a ground-shunt path. The conductor was actually found to be hanging in the air at a distance of about 8 km from the local terminal, proving this point.

During the arcing period, while the C-phase current magnitude dropped down, the magnitude of the ground current increased and, after about 125 ms from the start of the event, crossed the set threshold for the definite-time directional-overcurrent (67G) element. After a time delay of 10 cycles, 67GT picked up and the local relay sent a trip-permission signal to the remote end. At the remote terminal, 67G also picked up during the arcing period and then timed out for 67GT to pick up, causing the remote relay to send a trip-permission signal to the local relay. Upon receiving the trip-permission signal, the local relay tripped the line breakers and initiated the autoreclose scheme. The local relay reclosed the breaker after a set dead time of 2 s. However, while the C-phase conductor was hanging in the air by that time, the relay did not see any shunt fault and the line breakers remained closed until they were manually opened about six and a half minutes later.

The average value of the broken phase current was calculated to be 3.01 A primary in magnitude and $\angle 89.76°$ leading the broken phase voltage. This average value was calculated after the arc breaking point over 4 cycles, as shown by a dotted window in Fig. 19a.

2)   The Sequence of Events From the Remote End

Fig. 20 illustrates the event report captured by the remote relay at a sampling rate of 1,000 samples per second. We see that the remote relay also recorded the decrease in the amplitude of the broken-conductor phase, similar to what occurred at the local end. One of the zero crossings is the possible arc breakage point, and it is labeled as such. Beyond this point, the conductor is assumed to be broken. This is very likely because the C-phase current after this point is found to be capacitive and leading the C-phase voltage by about $\angle 90°$.

We calculated the average value of the broken-conductor current magnitude from the event report to be 69.15 A primary, and the average value of the current angle was $\angle 87.93°$ leading the corresponding phase voltage. This average value was calculated after the arc breaking point over 4 cycles, as shown by the dotted window in Fig. 20a.
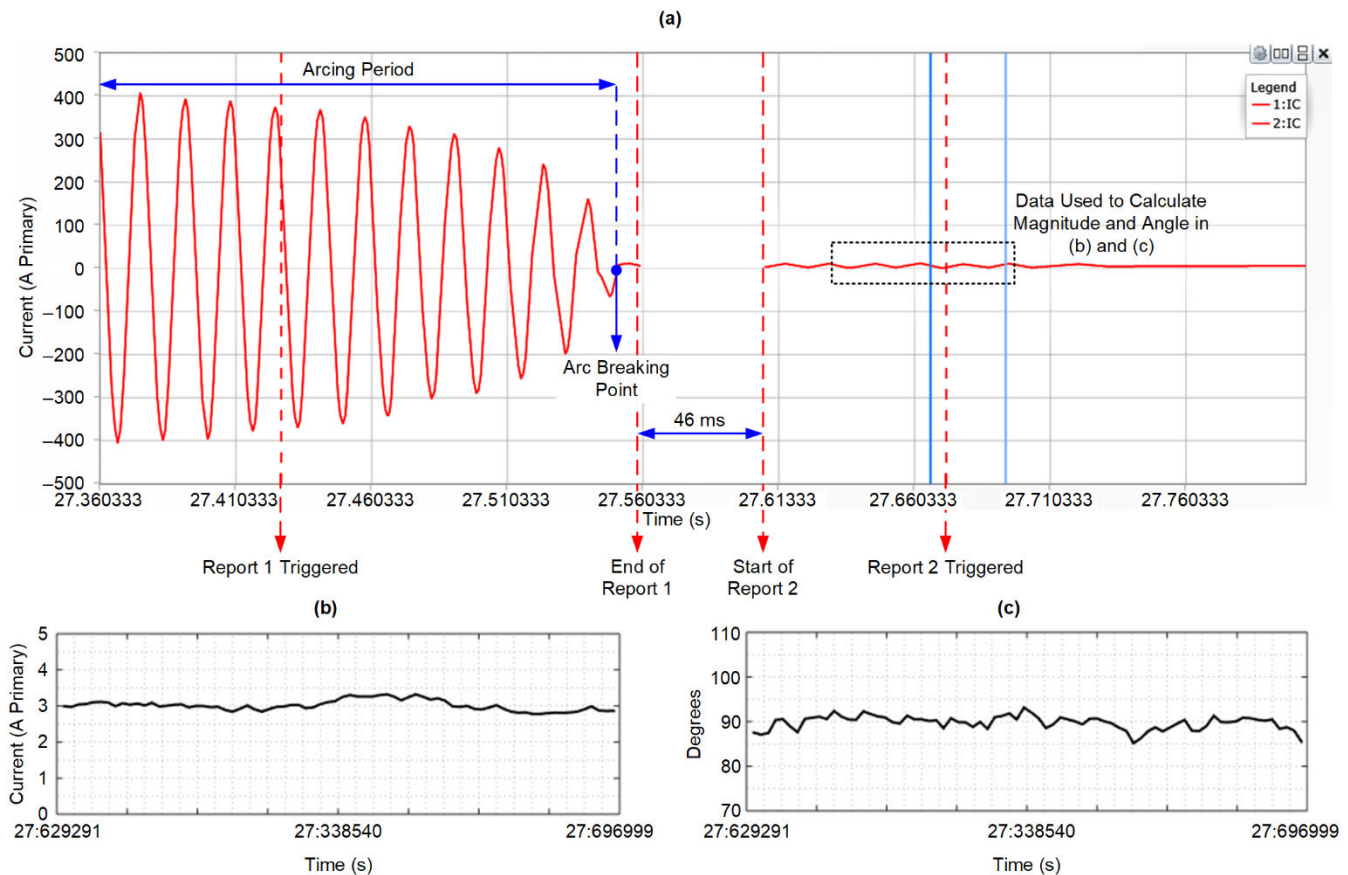
Fig. 19.   (a) Current waveform of the broken-conductor phase from two consecutive reports from the local relay; (b) magnitude of the broken-conductor phase current from the selected data in Report 2; (c) angle of the broken-conductor phase current with respect to the corresponding phase voltage from the selected data in Report 2.

During the arcing period, we see that the 67G2 picked up and before 67G2T could pick up, the remote relay already received the trip-permission signal from the local relay (see Fig. 20a). This caused the remote relay to trip the line breakers as soon as 67G2T picked up and to initiate the autoreclose scheme. The autoreclose dead time configured at this relay was 1 s. During this time, all the breakers at the local and remote ends were open. The C-phase conductor already broke and was hanging in midair from the local end. However, the conductor segment from the remote end fell to the ground. So, when the remote relay closed the breakers after the dead time, it closed on a C-phase ground fault. Fig. 21 illustrates the fault-current waveform when the breakers from the remote end were closed on the fault and tripped by the remote relay because of Zone 1 assertion of the distance element.

3)   Evaluation of the Proposed Algorithm

As mentioned in Section IV.A, we must know the total charging current of the protected line for the proposed algorithm to work. Because this is not known to us, the summation of the charging currents of the broken-conductor phase measured from the local and remote ends gives a good estimate of the total charging current, provided the voltage magnitudes at the local and remote ends are the same. Table I summarizes the 4-cycles average of the current and voltage magnitudes measured after the conductor breaks. Note that the local and the remote voltage magnitudes are not equal, so we normalize them to 1 pu and recalculate the corresponding charging currents. The summation of the recalculated charging currents is accurate enough to be considered the total charging current for C-phase.

TABLE I
AVERAGE VALUES OF THE VOLTAGE AND CURRENT MAGNITUDES
AFTER THE ARC BREAKING POINT

Terminal	Average Voltage Measured (pu)	Average Charging Current Measured (A)	Recalculated Values of Charging Current for 1 pu Voltage Magnitudes (A)
Local	0.73	3.01	4.15
Remote	1.01	69.15	68.44
Total			72.59
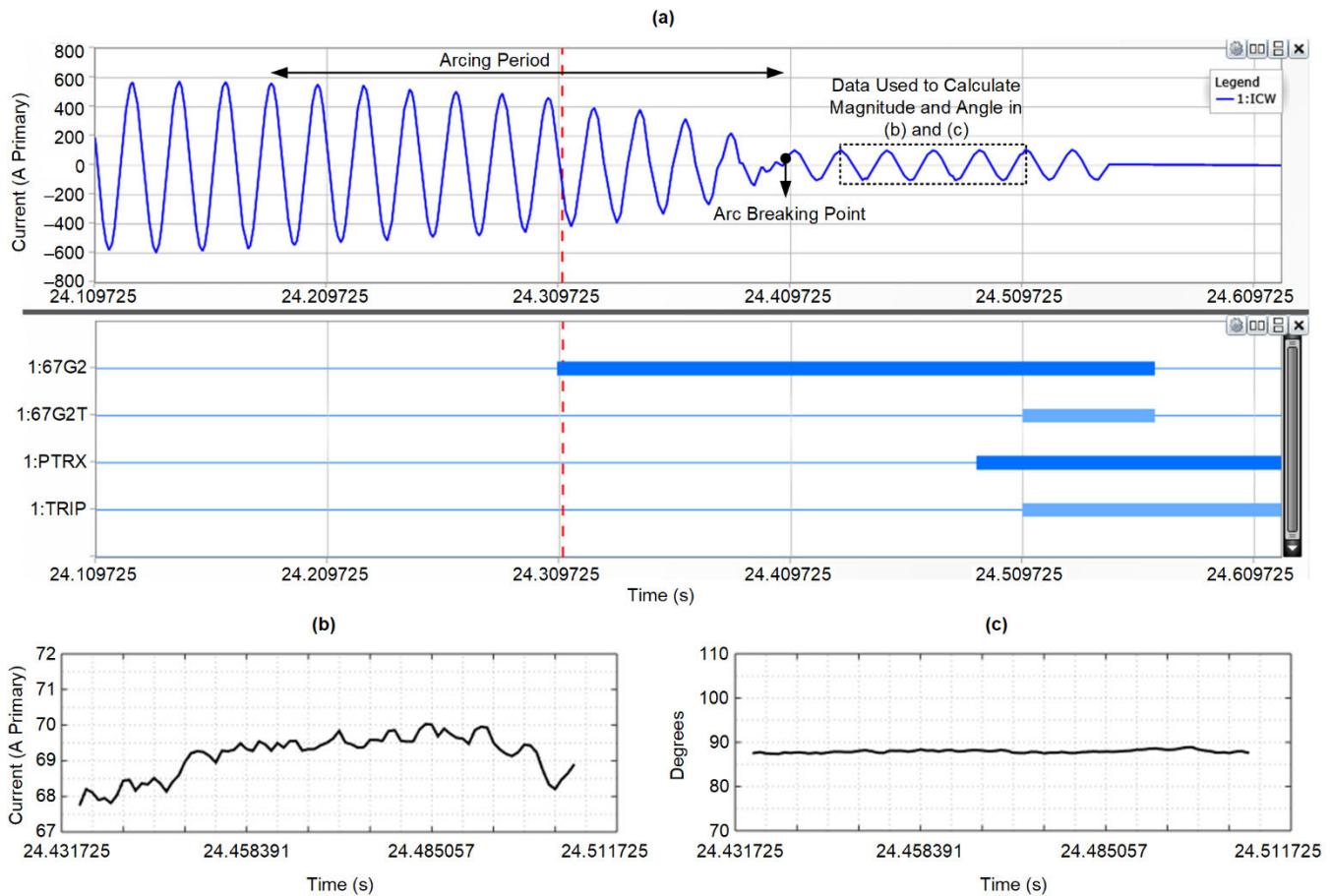
Fig. 20. (a) Current waveform of the broken-conductor phase from the remote relay; (b) magnitude of the broken-conductor phase current from the selected data; (c) angle of the broken-conductor phase current with respect to the corresponding phase voltage from the selected data.
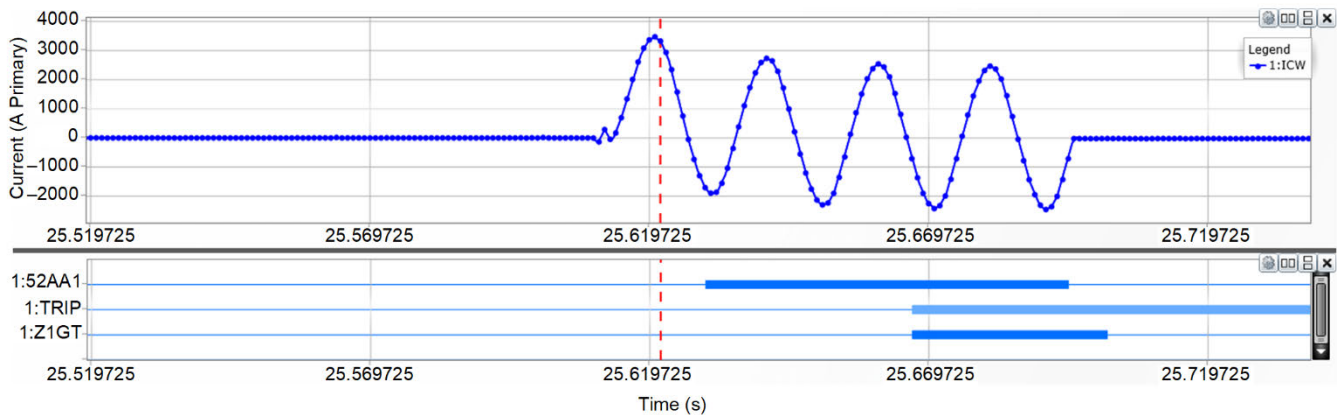
Fig. 21. Fault-current waveform when the breakers were closed on the fault from the remote end.

Because we now know the total charging current for the broken-conductor phase, we can test the proposed algorithm. All the criteria of the proposed algorithm are checked with the measured values at the local and remote terminals. Table II summarizes the results.

As we see in Table II, all the conditions of the proposed algorithm are satisfied at the local and the remote relays. If the proposed algorithm had been implemented, both the local and the remote relays would have detected a broken conductor within the zone of protection. Thus, they would not only have tripped the line breakers at both ends to prevent possible shunt

fault, but they also would have blocked autoreclose. In this event, the local and remote relays did trip, but they failed to block the autoreclose, and the remote relay experienced a C-phase shunt fault upon reclosing. The distance of the fault location calculated by the proposed algorithm is very close to the actual location that was observed during line inspection after the fault. The error is 0.24 km from the local end and 0.05 km from the remote end. The proposed algorithm is thus very beneficial in terms of protection as well as in locating broken-conductor faults.

TABLE II
PROPOSED ALGORITHM CRITERIA TESTED WITH THE MEASURED VALUES OF LOCAL AND REMOTE RELAYS

Criteria	Measured Values at the Local Relay	Pass/ Fail	Measured Value at the Remote Relay	Pass/ Fail
1. Magnitude Check: Phase magnitude must be less than the total charging current for the phase (72.59 A).	4.15 A	Pass	68.44 A	Pass
2. Angle Check: Phase angle must lead the respective phase voltage by more than $\angle 85°$ and less than $\angle 95°$.	$\angle 89.76°$	Pass	$\angle 87.93°$	Pass
3. Incremental-Angle Check: The incremental phase angle must be greater than $\angle 15°$ for forward power flow and smaller than $\angle -15°$ for reverse power flow (all angles are measured in the counterclockwise direction).	The angle of the C-phase current with relation to the C-phase voltage: Before the conductor breaks = $\angle 10°$, which indicates forward power flow. After the conductor breaks = $\angle 89.76°$, which indicates incremental-angle change = $\angle 79.76°$.	Pass	The angle of the C-phase current with respect to the C-phase voltage: Before the conductor breaks = $\angle 185°$, which indicates reverse power flow. After the conductor breaks = $\angle 87.93°$, which indicates incremental-angle change = $\angle -97.07°$.	Pass
4. Distance Check: Calculated distance should be less than the line length (144.193 km).	Using (2), calculated distance is 8.24 km.	Pass	Using (2), calculated distance is 135.95 km.	Pass

B. Field Event 2: A-Phase Broken-Conductor Event on a Tapped 57.1 kV Line

This section describes a broken-conductor field event of a 57.1 kV subtransmission line from Kauai Island Utility Cooperative (KIUC) in Hawaii. As shown in Fig. 22, the total length of the line is 16.75 mi, and there is a tap load 10.75 mi from the Lihue terminal. The A-phase conductor broke between the Lawai tap and Lihue terminal and was hanging in midair from the Lihue terminal end while the conductor segment from the Port Allen terminal end hit a ground structure, creating a shunt fault. We calculated the location to this shunt fault by using traveling waves and determined that it was 6.96 mi from the Port Allen terminal. If we consider this fault location as the broken-conductor fault location, the distance to the broken conductor from the Lihue terminal is 16.75 – 6.96 = 9.79 mi. The broken conductor was actually located approximately 10.02 mi from the Lihue terminal.
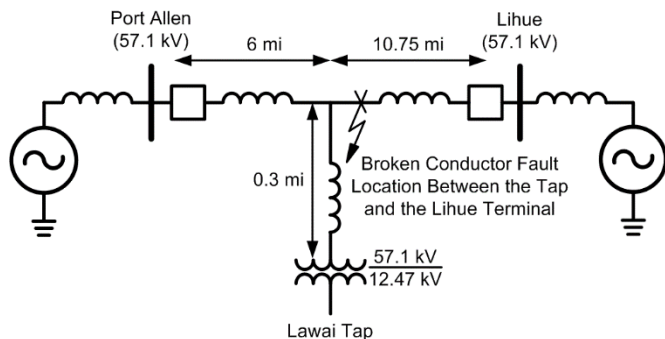
Fig. 22. Broken-conductor field event of a 57.1 kV subtransmission line from KIUC in Hawaii.

Fig. 23 depicts the A-phase current and voltage as measured by the relay at Lihue terminal at the rate of 10,000 samples per second. Note that the event reports at the Lihue and Port Allen terminal relays were triggered when the conductor segment from the Port Allen end caused the ground fault. According to the utility records, the conductor broke 1.7 s before the shunt fault, and as such, there is no capture of the series arcing that might have occurred during the conductor break. Also, because the A-phase broken conductor was hanging in the air from the Lihue side, the relay at that terminal measured the shunt capacitance current accounting to the length of the line from the Lihue bus to the hanging broken conductor. We calculated the average value of the phase current of the broken conductor from the Lihue terminal to be 2.15 A primary in magnitude and $\angle 92.67°$ leading the broken-conductor phase voltage. We calculated this average value over the period of 4 cycles, as shown by a dotted window in Fig. 23. The disturbance shown around 10.58 s is because of the coupling effect from B- and C-phases, which were in turn affected by traveling waves launched by the A-phase-to-ground fault from the Port Allen end.

The total charging current per phase for this line was calculated to be 3.48 A primary using (1). The characteristic impedance (Z_1) and propagation constant (γ_1) for (1) are calculated by using the line parameters and the traveling-wave propagation time setting, which we acquire from the event report of the relay. Appendix B provides the details of this calculation.

Because we now know the total charging current per phase, we can test the proposed algorithm. Table III summarizes the results for the proposed algorithm at the Lihue terminal. Note that the zone of protection is considered to be the entire line from the Port Allen terminal to the Lihue terminal, ignoring the Lawai tap. It may appear that there should be two protection zones, one from the Port Allen terminal to the tap, and another from the Lihue terminal to the tap; however, ignoring the tap does not create any security issues even though it does decrease dependability. For example, if there is a broken conductor between the tap and the Lihue terminal, the current measured at the Port Allen terminal would not be purely capacitive because of the tap load, and the proposed algorithm would not trigger.
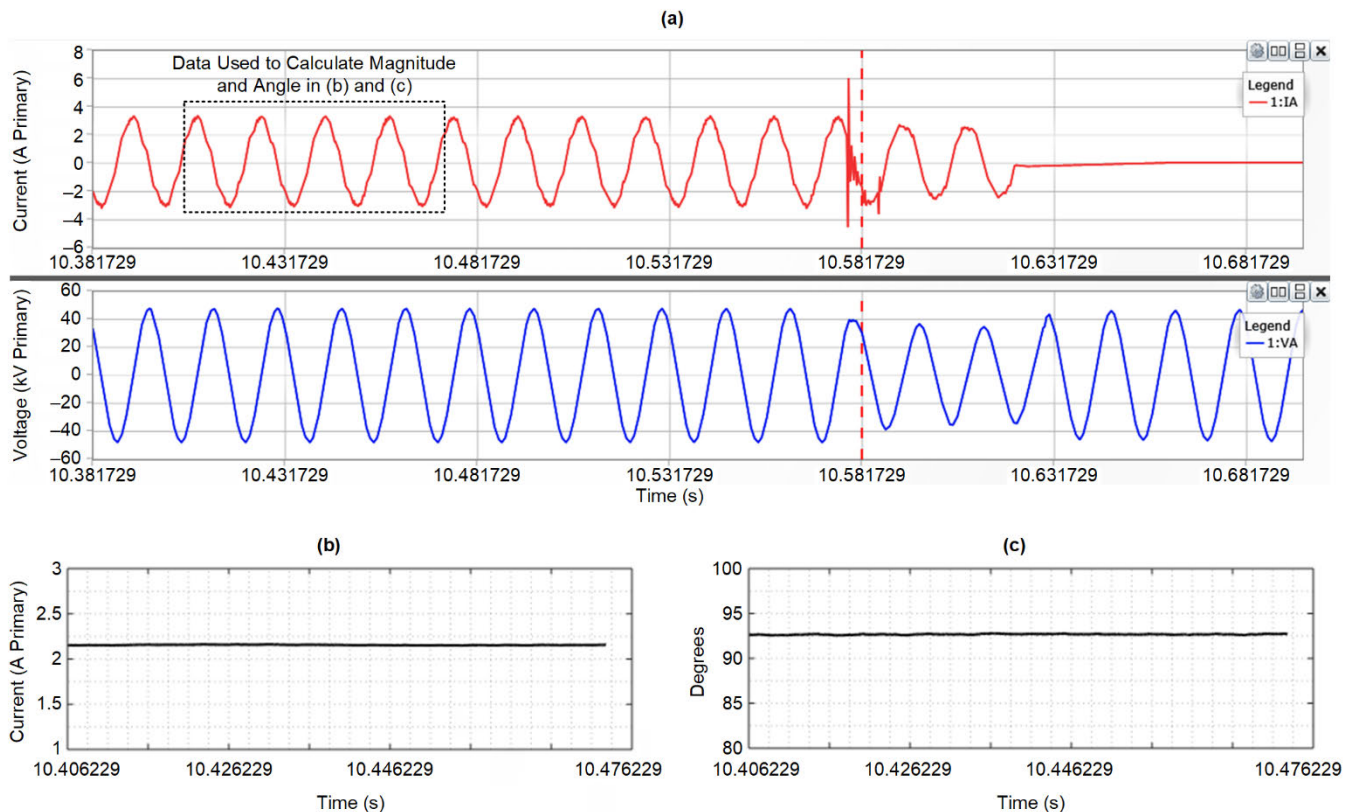
Fig. 23. (a) Current waveform of the broken-conductor phase from the relay at the Lihue terminal; (b) magnitude of the broken-conductor phase current from the selected data in the report; (c) angle of the broken-conductor phase current with respect to the corresponding phase voltage from the selected data in the report.

TABLE III
PROPOSED ALGORITHM CRITERIA TESTED WITH MEASURED VALUES
AT LIHUE TERMINAL

Criteria	Measured Values at the Local Relay	Pass/Fail
1. Magnitude Check: Phase magnitude must be less than the total charging current for the phase (3.48 A).	2.15 A	Pass
2. Angle Check: Phase angle must be leading the respective phase voltage by more than $\angle 85°$ and less than $\angle 95°$.	$\angle 92.67°$	Pass
3. Incremental-Angle Check: The incremental phase angle must be greater than $\angle 15°$ for forward power flow and smaller than $\angle -15°$ for reverse power flow (all angles are measured in the counterclockwise direction).	There were no data captured before the conductor broke, so this criterion cannot be tested.	NA
4. Distance Check: Calculated distance should be less than the line length (16.75 mi).	Using either (2) or (11), calculated distance is 10.35 mi.	Pass

Table III shows three of the four conditions of the proposed algorithm satisfied. The third criterion, the incremental phase angle check, cannot be tested because there were no data captured before the conductor broke. However, the power flow directions of the B-phase and C-phase after the A-phase conductor break were in the forward direction because their phase currents were leading corresponding phase voltages by approximately $\angle 39°$ and $\angle 15°$, respectively. Assuming the power flow direction has not changed before and after the broken-conductor fault, we can safely say that the power flow direction of the A-phase conductor before the conductor break was in the forward direction. With this assumption, the incremental current phase angle would be positive and above the $\angle 15°$ threshold, satisfying the third criterion. Thus, the proposed algorithm would have detected the broken-conductor fault condition within the zone of protection, and, if configured, would have tripped the line breakers and blocked the autoreclose. The distance to the broken-conductor fault, as calculated by the proposed algorithm, is 10.35 mi from the Lihue terminal. The distance calculated through the traveling waves captured at Port Allen caused by the shunt fault is 9.79 mi from the Lihue terminal. The broken conductor was actually found to be around 10.02 mi from Lihue terminal. Considering this as the reference fault location, the proposed algorithm has an error of 0.33 mi in estimating the broken-conductor fault location.

From the Port Allen terminal, the conductor broke and was in the air for about 1.7 s before touching the ground. This means that the current shown in Fig 24 before the shunt fault is drawn by the tap load, as the connection between the Port Allen terminal and the Lawai tap was still intact. The tap load on A-phase was 14.2 A $\angle 5.9°$ primary.
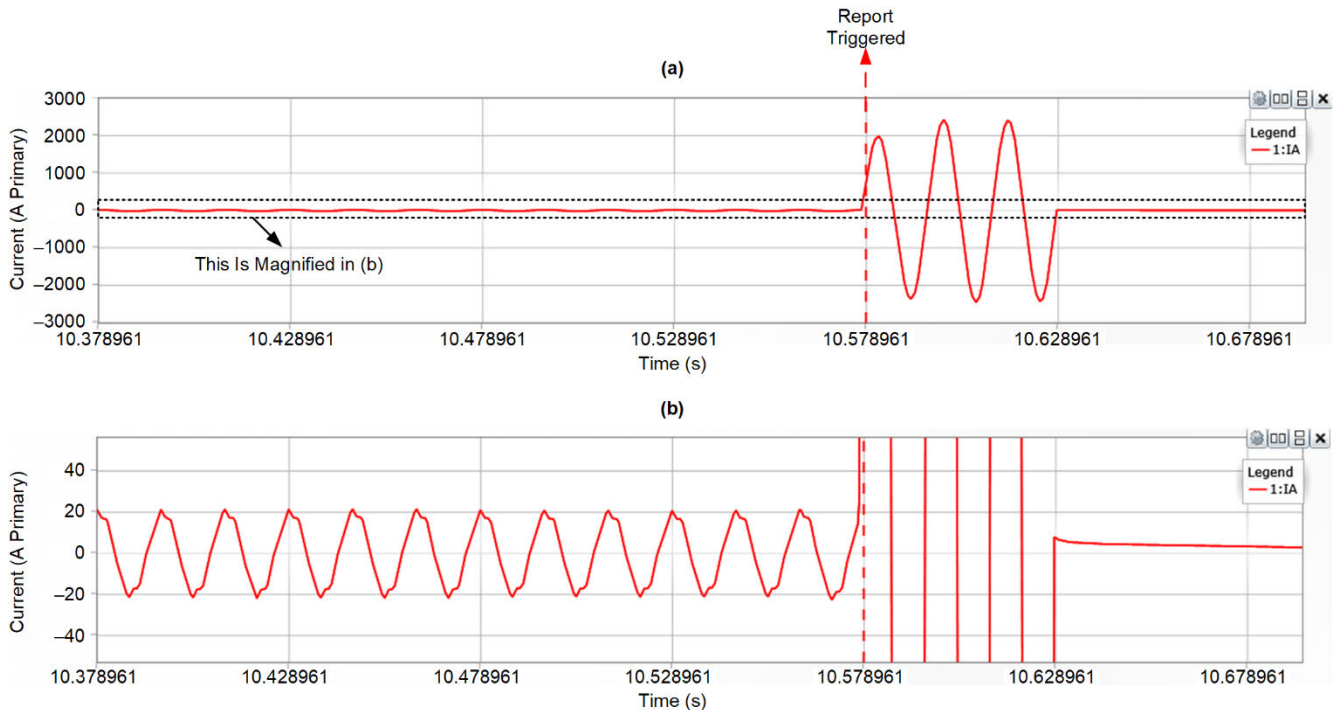
Fig 24.　Current waveform of the broken-conductor phase from the relay at the Port Allen terminal, (a) normal scaling and (b) zoomed in.

During the 1.7 s when the conductor was falling through the air to the ground, the relay would have measured the capacitance current from the Port Allen terminal to the broken-conductor location, but this current was superimposed with the current drawn by the load at the Lawai tap. Because of this, none of the criteria of the proposed algorithm would have been satisfied, and the broken conductor from the Port Allen terminal would not have been detected. In cases like these, we can use the direct-transfer trip from the Lihue terminal based on the broken-conductor detection to trip the line breakers at the Port Allen terminal and prevent the shunt fault.

C. Field Event 3: Close-In Broken-Conductor Event on a 220 kV Double-Circuit Line

This section explains a broken-conductor field event that occurred in a 220 kV parallel-line system [3]. The A-phase jumper of Line 1, which was connected to the wave trap at the local substation, snapped and remained hanging in the air. This resulted in a diversion of the load from the Line 1 A-phase conductor to the Line 2 A-phase conductor. Relays on both of the parallel lines calculated the circulating ground currents, which exceeded the set threshold for the ground-current element. The configured directional ground-current element picked up for Line 2 but not for Line 1. This was because the Line 1 relay declared the ground-current direction as reverse, whereas the Line 2 relay declared it as forward and tripped. In [3], there are no recordings of this event, so we created a similar event by using a two-machine system with a line length of 90 mi, as shown in Fig. 25.

We simulated a broken-conductor fault on Line 1 close to the breaker. Before the conductor broke, both parallel lines were equally loaded as shown in Fig. 26. All the phasor values are in pu, with voltage base as 220 kV and current base as

250 A. The voltage and the current phasors are not perfectly balanced because of the untransposed nature of the line and the slightly unbalanced load, which are typical in transmission systems. We tested the protection scheme for the ground-overcurrent directional element with a ground-current pick up of 0.5 pu.
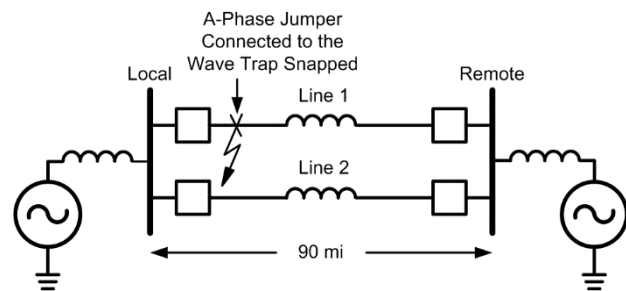
Fig. 25.　Broken-conductor field event in a parallel-transmission-line system.
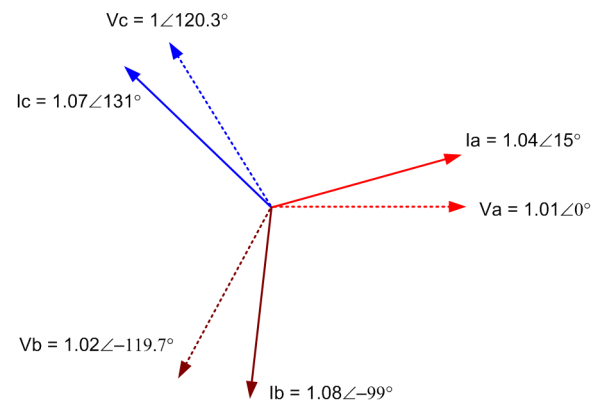
Fig. 26.　Phase currents and voltages of Line 1 and Line 2 before the conductor broke in Line 1.

After the A-phase conductor of Line 1 broke close to the breaker, the current measured through it by the local relay became 0 pu, whereas the current in the A-phase conductor of Line 2 increased, as shown in Fig. 27. As expected, the magnitude of the ground current calculated by the relays on Line 1 and Line 2 increased as shown in Fig. 28 and crossed the set threshold of 0.5 pu.
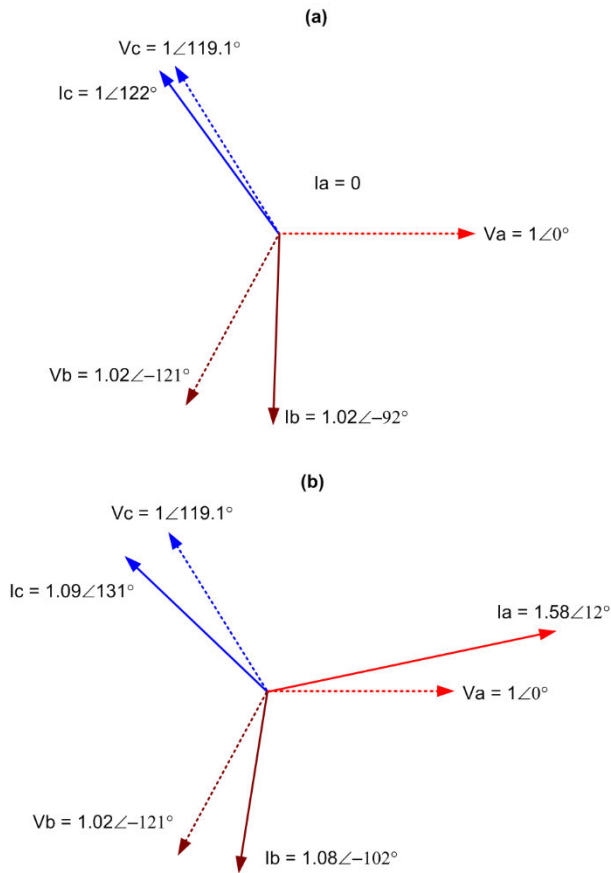
Fig. 27. Phase voltages and currents after the conductor broke on Line 1 (a) for Line 1 (b) for Line 2.

The directional elements are typically set to operate for shunt faults and are not meant for series faults like a broken conductor. For the zero-sequence impedance-based directional elements, if the zero-sequence impedance calculated by the relay is positive and greater than a certain threshold (e.g., 0.3 Ω secondary), the fault direction declaration is reverse, and if it is negative and less than a certain threshold (e.g., −0.3 Ω secondary) the fault declaration is forward [4]. The same is true if the direction is determined using negative-sequence impedance. For this simulation, we used a directional element based on the zero-sequence impedance calculation. We see in Fig. 28, that for Line 1, the relay declared a reverse direction because the calculated zero-sequence impedance was positive and did not trip the local breaker, while the relay on Line 2 declared a forward direction because the calculated zero-sequence impedance was negative and tripped the Line 2 breakers.

From this event, we can conclude that the security of the directional elements is uncertain for series faults, and if the overcurrent element picks up, the direction can lead to an unintended trip of a parallel line without a fault.

When a conductor breaks very close to the relay location, the charging current measured by the relay would be close to 0 A. The relay cannot calculate angles of such small magnitudes of currents, so the phase current angle and phase current incremental-angle checks of the proposed algorithm cannot be evaluated. To detect broken conductors under such scenarios, we need a different approach, which was outlined in Section V. However, even if the broken-conductor fault is detected in the protected line, it is still challenging to protect the parallel line, which has sensitive 67GT, 67QT, or 67PT elements. If these elements are time-delayed by about 400 ms and get blocked by the broken-conductor detection or pole-open condition from the relay on the protected line, then the misoperation can be prevented.
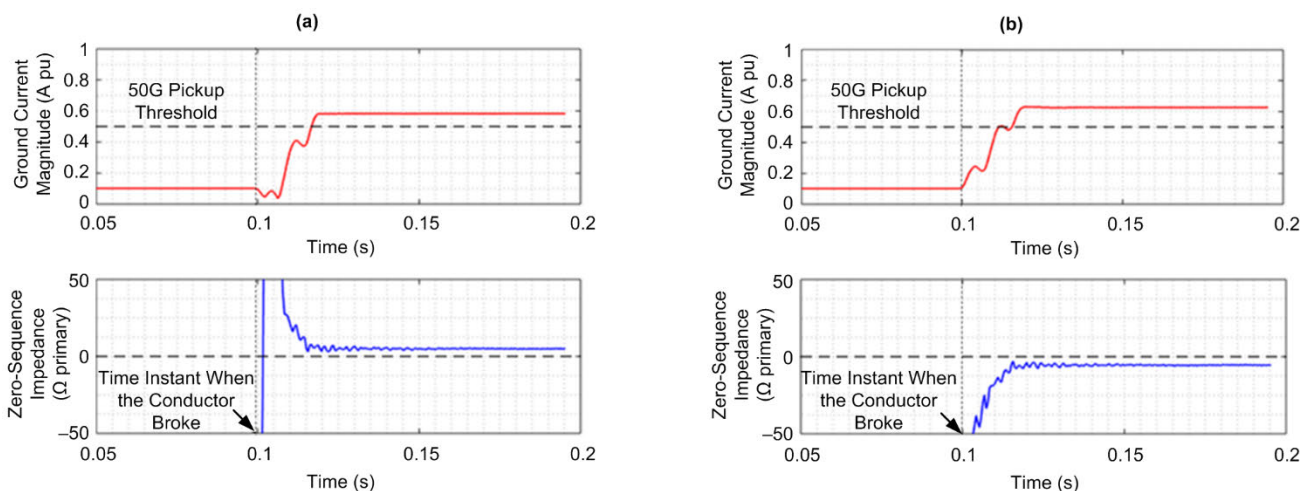
Fig. 28. The ground-current magnitude and calculated zero-sequence impedance by relays at (a) Line 1 (b) Line 2.

IX. Conclusion

Traditionally, the $|I_2/I_1|$ threshold check with a time delay has been used to detect broken conductors. This paper explains the selectivity issues and the security concerns of using $|I_2/I_1|$ during low loads and the challenges in time coordination for meshed systems. Furthermore, a significant time delay is set, which is in the order of tens of seconds, that would neither prevent the shunt faults nor block the autoreclose if the broken conductor converts into a shunt fault.

We propose a new algorithm for detecting and locating broken conductors. It is suitable for lines with measurable total charging current, even if it is as low as 2 A primary. Also, the algorithm is immune to loading conditions and can be implemented on single-circuit lines, parallel lines, lines with shunt reactors, and lines with tap loads. The proposed method can detect broken conductors when the conductor breaks and remains in physical isolation with the ground path for a minimum amount of time (e.g., 4 cycles). This time is used to ascertain that the relay is measuring steady-state charging current or, in the case of a broken conductor very close to the relay, no current.

We performed extensive EMTP simulations to test the algorithm on a 90-mile single-circuit and a 135-mile double-circuit line. The algorithm successfully detected the broken-conductor faults in these lines. This paper proposes three methods to calculate the distance to the broken-conductor fault, namely, current ratio, positive-sequence, and complete equation methods. Simulation results for a 90 mi single-circuit line show that all three methods have errors less than 2 mi for a broken-conductor fault anywhere along the length of the line. For a 135 double-circuit line, the errors increase with increasing fault distance because of mutual coupling between the parallel lines, but the errors were found to be within 6 mi.

For calculating the fault location, the current ratio method is the simplest in terms of computational complexity, followed by the positive-sequence method, which requires positive-sequence line parameters. The complete equation method does not have a closed-form solution and must be solved iteratively. Additionally, it also requires zero-sequence parameters, which are often not accurately known. This paper explains that the difference between the positive-sequence and the complete equation is minimal, diminishing the need to perform complex iterations for similar results. Therefore, for single-circuit lines, we can use either one of the location methods—current ratio or positive-sequence. However, for double-circuit lines, it is preferable to use the positive-sequence method because the errors are consistent and tend to underreach, as opposed to the current ratio method, where the error is unpredictable and depends on the load current on the parallel line.

We analyzed three broken-conductor field events and successfully validated the proposed algorithm for them. For Field Events 1 and 2, it would have taken around 350 ms and 160 ms, respectively, to declare a broken-conductor fault. In other words, the proposed algorithm can detect the broken-conductor faults within 400 ms of mechanical breakage of the conductor. It depends, of course, on how long the arc takes to extinguish, which can increase or decrease this detection time.

Detecting broken conductors within 400 ms allows the relay to prevent shunt faults if the conductor eventually falls to the ground and can prevent faults by blocking the autoreclose, thus reducing further stress on the system. A broken conductor is assumed to take at least 1 s of free-falling towards the ground. In Field Event 2, it took around 1.7 s.

We know that directional elements are not reliable for series faults because they are designed to operate for shunt faults. Using sensitive directional-overcurrent elements can lead to misoperations, as seen in the parallel lines of Field Event 3. One option to avoid such misoperations on a healthy line is to configure such sensitive elements with a time delay during which the proposed algorithm can detect a broken conductor on the faulted line and send a signal to block the ground element on the parallel healthy line.

X. Appendix A: Simulation Model Details

TABLE IV
LOCAL AND REMOTE SOURCE PARAMETERS FOR SINGLE- AND DOUBLE-CIRCUIT MODELS

Source Parameters	Local Source	Remote Source
Line-to-line voltage for single-circuit model (kV)	$132\angle 20°$	$132\angle 0°$
Line-to-line voltage for double-circuit model (kV)	$220\angle 24°$	$220\angle 0°$
Total positive-sequence impedance (Ω)	$15.88\angle 80°$	$35.59\angle 65°$
Total zero-sequence impedance (Ω)	$230\angle 77.47°$	$69.06\angle 65°$
Frequency (Hz)	60	60

TABLE V
OVERHEAD LINE PARAMETERS FOR THE SINGLE-CIRCUIT MODEL

Line Parameters	Values
Positive-sequence impedance per mile (Ω)	$0.7585\angle 81.60°$
Zero-sequence impedance per mile (Ω)	$2.6130\angle 81.45°$
Positive-sequence shunt capacitance per mile (nF)	15.31
Zero-sequence shunt capacitance per mile (nF)	8.76
Total line length (mi)	90
Transposition cycle (mi)	45
Inner radius of phase conductor (in)	0
Outer radius of phase conductor (in)	0.588
DC resistance of phase conductor per mile (Ω)	0.108
Number of bundled conductors per phase	1
DC resistance of shield conductor per mile (Ω)	1.108
Horizontal tower configuration for A-, B-, and C-Phases (ft)	25.59, 0, and 22.31
Vertical tower configuration for A-, B-, and C-Phases (ft)	42.651, 49.213, and 55.774
Vertical midspan configuration for A-, B-, and C-Phases (ft)	28.43, 32.808, and 37.183
Soil resistivity (Ωm)	100

TABLE VI
OVERHEAD LINE PARAMETERS FOR THE DOUBLE-CIRCUIT MODEL

Line Parameters	Values
Protected Line	
Positive-sequence impedance per mile (Ω)	$0.77\angle 81.69°$
Zero-sequence impedance per mile (Ω)	$1.79\angle 78.98°$
Positive-sequence shunt capacitance per mile (nF)	15.26
Zero-sequence shunt capacitance per mile (nF)	9.51
Total line length (mi)	135
Transposition cycle (mi)	45
Inner radius of phase conductor (in)	0
Outer radius of phase conductor (in)	0.588
DC resistance of phase conductor per mile (Ω)	0.108
Number of bundled conductors per phase	1
Inner radius of shield conductor (in)	0
Outer radius of shield conductor (in)	0.413
DC resistance of shield conductor per mile (Ω)	0.254
Horizontal tower configuration for A-, B-, and C-Phases and shield (ft)	3.999, 0, 5.167, and 15.417
Vertical tower configuration for A-, B-, and C-Phases and shield (ft)	49.341, 61.506, 76.007, and 80.712
Vertical midspan configuration for A-, B-, and C-Phases and shield (ft)	32.894, 41.004, 50.671, and 53.808
Soil resistivity (Ωm)	100
Parallel Line	
Positive-sequence impedance per mile (Ω)	$0.77\angle 81.69°$
Zero-sequence impedance per mile (Ω)	$1.79\angle 78.69°$
Positive-sequence shunt capacitance per mile (nF)	15.268
Zero-sequence shunt capacitance per mile (nF)	9.514
Total line length (mi)	135
Transposition cycle (mi)	45
Inner radius of phase conductor (in)	0
Outer radius of phase conductor (in)	0.588
DC resistance of phase conductor per mile (Ω)	0.108
Number of bundled conductors per phase	1
Inner radius of shield conductor (in)	0
Outer radius of shield conductor (in)	0.413
DC resistance of shield conductor per mile (Ω)	0.254
Horizontal tower configuration for A-, B-, and C-Phases and shield (ft)	26.834, 30.833, 25.666, and 15.417
Vertical tower configuration for A-, B-, and C-Phases and shield (ft)	49.341, 61.506, 76.007, and 80.712
Vertical midspan configuration for A-, B-, and C-Phases and shield (ft)	32.894, 41.004, 50.671, and 53.808
Soil resistivity (Ωm)	100
Zero-sequence transfer impedance per mile (Ω)	$1.027\angle 76.95°$

XI. APPENDIX B: TOTAL LINE-CHARGING CURRENT FOR FIELD EVENT 2

TABLE VII
STEPS FOR CALCULATING THE TOTAL LINE-CHARGING CURRENT OF THE LINE FOR FIELD EVENT 2

Line Parameters	Values
*System frequency (Hz)	60
*System line-to-line voltage, V_{LL} (kV)	57.1
*Total line length (mi)	16.75
*Traveling-wave propagation time for the complete line length, TWPT (μs)	95
*Total positive-sequence impedance of the line, Z_1 (Ω primary)	$12.86\angle 74.3°$
Total positive-sequence inductance of the line, L_1 (mH primary)	$L_1 = \dfrac{\operatorname{Im}ag[Z_1]\cdot 10^3}{2\pi\cdot \text{Freq}} = 32.8$
Total positive-sequence capacitance of the line, C_1 (nF primary)	$C_1 = \dfrac{\text{TWPT}^2}{L_1} = 274.82$
Positive-sequence characteristic impedance of the line, Z_{C1} (Ω primary)	$Z_{C1} = \sqrt{\dfrac{Z_1}{1j\cdot 2\pi\cdot \text{freq}\cdot C_1}}$ $Z_{C1} = 352\angle -7.85°$
Total positive-sequence propagation constant of the line, γ_1	$\gamma_1 = \sqrt{Z_1\cdot 1j\cdot 2\pi\cdot \text{freq}\cdot C_1}$ $\gamma_1 = 0.0365\angle 82.15°$
Total capacitance current of the line when using (1)	$I_C = \dfrac{V_{LL}}{\sqrt{3}}\dfrac{\tanh(\gamma_1)}{Z_{C1}} = 3.48\angle 90°$

* From relay settings

XII. ACKNOWLEDGMENT

XIII. REFERENCES

[1] Transpower New Zealand Limited, "TL Conductors and Insulators Fleet Strategy," Document TP.FL 01.00, October 2013. Available: https://www.transpower.co.nz/node/10951/fleet-strategies.

[2] J. J. Grainger and W. D. Stevenson, Jr., "Current and Voltage Relations on a Transmission Line," *Power System Analysis*. Edition 2003. Tata McGraw Hill, New Delhi, India, 1994, pp. 193–237.

[3] V. H. Manohar, N. Sankaranarayanan, and K. Jagannath, "Directional Earth Fault Protection for Transmission Lines – Need and Operational Experiences," proceedings of the Fifteenth National Power Systems Conference, Powai, India, December 2008.

[4] K. Zimmerman and D. Costello, "Fundamentals and Improvements for Directional Relays," proceedings of the 63rd Annual Conference for Protective Relay Engineers, College Station, TX, March 2010.

XIV. BIOGRAPHIES

Kanchanrao Dase received his B.E. degree in electrical engineering from Sardar Patel College of Engineering, University of Mumbai, India, in 2009. He received his M.S. degree in electrical engineering from Michigan Technological University in Houghton, MI, in 2015. From 2009 to 2014, he was a manager at Reliance Infrastructure Limited with a substation engineering and commissioning profile. Currently, he is working with Schweitzer Engineering Laboratories, Inc. as a power engineer. His research interests include power system protection, substation automation, and fault locating.

Sajal Harmukh received his B.Tech degree in electrical power engineering in 2012 from the Indian Institute of Technology Delhi in India, and his M.S. degree in electrical engineering in 2016 from the University of Illinois at Urbana-Champaign in Champaign, IL. Previously, he worked for NTPC Limited, India, as an assistant manager in the Operations and Maintenance department. He currently works as a power engineer at Schweitzer Engineering Laboratories, Inc.

Arunabha Chatterjee received his B.Tech degree in electrical and electronics engineering from the National Institute of Technology Karnataka in Mangalore, India, in 2014. He received his M.S. degree in electrical and computer engineering from Georgia Institute of Technology in Atlanta, GA, in 2015. Since 2016, he has been working as a power engineer at Schweitzer Engineering Laboratories Inc.